Journal of
Water & Climate Change

IWA PUBLISHING

Journal of Water and Climate Change Vol 12 No 8, 3602 doi: 10.2166/wcc.2021.398

Singular value decomposition (SVD) based correlation analysis of climatic factors and extreme precipitation in Hunan Province, China, during 1960–2009

Hui Zhou [b], Junjun Zhu [a,*], Heng Xiao [c] and Xinkui Wang [d]

[a] College of Resources and Environment Science, South-Central University for Nationalities, Wuhan 430074, China
[b] Hunan Hydrology and Water Resources Center, Changsha 410007, China
[c] School of Environmental and Municipal Engineering, North China University of Water Resources and Electric Power, Zhengzhou 450046, China
[d] College of Hydrology and Water Resources, Hohai University, Nanjing 210098, China
*Corresponding author. E-mail: junjunzhu@mail.scuec.edu.cn

HZ, 0000-0002-1123-1619; HX, 0000-0001-6131-1433

ABSTRACT

A small change in the mean climate may lead to a dramatic change in the frequency and intensity of extreme climate events. In this study, the relationship between mean temperature (MT) and extreme precipitation and the influence from large-scale circulation were investigated in Hunan Province. The correlation between MT and the frequency of extreme precipitation events in different seasons (spring, summer, and autumn) and time periods (1960–2009) was used to obtain pairs of spatial patterns by the singular value decomposition method. The temporal expansion series displayed a consistent trend of temperature and extreme precipitation, and a mutation was observed to occur approximately during the 1980s–1990s. Temperature exhibited a warming trend after the mutation, but the frequency of extreme precipitation events exhibited obvious spatio-temporal variations. The causes of seasonal differences in the frequency of extreme precipitation events were determined by comparing interdecadal changes in three atmospheric circulation factors (850 hPa winds, the entire layer of vapor transportation fluxes and vapor flux divergence) before and after the mutation was revealed.

Key words: climate index, extreme precipitation, Hunan Province, singular value decomposition (SVD)

HIGHLIGHTS

- The relationship between temperature and extreme rainfall events was investigated using the SVD method.
- The temperature exhibited a sudden change during the 1980s–1990s.
- The trend of temperature change was widely varied.
- The correlation between temperature and extreme rainfall exhibited a significant spatial variation.
- The wind anomaly field revealed the opposite trends before and after the abrupt change.

1. INTRODUCTION

With global warming as the main feature, climate change has become a global environmental problem (Ye *et al.* 2013), significantly affecting social and economic development (Deng & Chen 2017). The report of the first working group of the fifth assessment report (AR5) issued by the Intergovernmental Panel on Climate Change (IPCC 2013) pointed out that the global temperature increased by 0.85 °C during 1880–2012, and the surface temperature has been warmer in the past three decades than in any decade since 1850. Under the background of global warming, the intensity of water cycle may increase, and the temporal and spatial distributions of global and regional precipitation have changed significantly (Douville *et al.* 2012). The response of regional precipitation to climate change and its cause analysis have become a relevant issue in current scientific research. In particular, extreme precipitation events are of global concern (Dai *et al.* 1998; Groisman *et al.* 1999; Frich *et al.* 2002), and they have been drawing increasingly more attention in China as well (Wang *et al.* 2012; Chen *et al.* 2016). To better understand changes in extreme precipitation events, many scholars have considered the correlation between extreme precipitation and temperature (Allen & Ingram 2002; Pumo *et al.* 2019; Gao *et al.* 2020).

Hunan Province is located in the southern part of the middle reaches of the Yangtze River, which belongs to a typical continental subtropical monsoon humid climate zone. Located at the intersection of southeast monsoon and southwest monsoon, the distribution of precipitation is uneven, with a large inter-annual variation (Wu *et al.* 2020). In recent years, abnormal precipitation events during the flood season and frequent drought and flood disasters in Hunan Province have significantly affected the national economic production of China (Cai *et al.* 2019). Therefore, studying the spatio-temporal variation of extreme precipitation events has high significance in flood control management and sustainable utilization and rational allocation of water resources in Hunan Province. The trend of precipitation in China has been found to be seasonally dependent. In Northeast China, North China and Central China, precipitation exhibits decreasing trends mainly in spring and autumn. In contrast, precipitation has been recorded to exhibit increasing trends throughout the year in most regions in Northwest China (Gemmer *et al.* 2004; Wang & Zhou 2005). Therefore, extreme precipitation events in China show regional and temporal differences. Precipitation events are increasing in the south of the Yangtze River, but decreasing in North China (Zhang *et al.* 2011). Moreover, summer extreme precipitation events are increasing in Western China but decreasing in North China and Northeast China (Wang & Zhou 2005; Ning & Qian 2009).

Previous studies analyzed the correlation between climate change and extreme precipitation, generally focusing on the frequency, intensity, and total amount of extreme precipitation to annual precipitation (Manton *et al.* 2010; An *et al.* 2020). According to the Clausius–Clapeyron (C–C) relationship, the frequency of extreme precipitation events increases with global warming (Allen & Ingram 2002; Gao *et al.* 2018). However, many studies reported that the relationship is not always consistent with the C–C relationship and exhibits spatio-temporal variations (Berg *et al.* 2009; Ali *et al.* 2018). The linear regression, Mann–Kendall (MK), and slope estimation methods are also commonly used for determining the temporal variation trend of extreme precipitation. The extreme climate index is used to represent extreme climate conditions. The Expert Team on Climate Change Detection and Indexes (ETCCDI) defined and recommend 27 extreme climate indices for evaluating regional extreme climate conditions (Lupikasza 2009). These indices comprise 11 extreme rainfall indices and 16 extreme temperature indices. The extreme precipitation indices have been widely used to study the temporal variation trend of extreme precipitation (Baidya *et al.* 2008; Lupikasza 2009).

The frequency of extreme rainfall events is expected to increase in the future, and neglecting these changes will result in the underestimation of extreme events (Oruc 2021). To investigate the trend of extreme rainfall events, various methods such as MK, moving *t*-test technique Cox–Stuart, and Pettitt's (P) tests have been applied, and nonstationary generalized extreme value models have been developed (Wu *et al.* 2015). However, most previous studies focused only on a certain aspect of precipitation regimes, such as precipitation means (Jiang *et al.* 2007; Chen *et al.* 2014), precipitation maxima (Lü *et al.* 2018), or selected only a limited number of precipitation indices (Guo *et al.* 2013; Zhang *et al.* 2013). In the research of climate change, global climate model and regional climate model datasets have been used to determine the intensity and frequency of precipitation, which may become more critical in the late 21st century (Singh & Xiaosheng 2019; Sharma & Goyal 2020).

Climate change may be identified earlier than other variables in some variables, which is partly because extreme values are directly related to abnormal weather phenomena, but common climate elements are expressed in the form of monthly or seasonal average. There is little research on the relationship between mean temperature (MT) and extreme precipitation. However, some studies have shown that the mean change in the original field of climate elements can lead to a nonlinear change in the frequency and intensity of extreme climate events, that is, a small change in the mean climate may lead to a dramatic change in the frequency and intensity of extreme climate events. Meanwhile, the relationship between the change of extreme precipitation and the general circulation situation is also important.

In view of the above, the objective of this study was to investigate the relationship between MT and extreme precipitation and the influence from large-scale circulation. A singular value decomposition (SVD) analysis was used to obtain pairs of spatial patterns between MT and extreme precipitation that were optimally correlated. SVD is a factorization of a rectangular matrix, which has been mostly applied to investigate inter-relationships between two spatial–temporal variables (Ghajarnia *et al.* 2016; An *et al.* 2020). The findings of this study can further improve our understanding of the changing characteristics of extreme precipitation induced by probable climate drivers in different seasons and different parts of Hunan Province with temperature change. Moreover, they can provide some guidance for the construction of reasonable flood control management strategies and water resource utilization projects in Hunan Province.

2. MATERIALS AND METHODS

2.1. Study area

Hunan Province is located in Central China (24°38′–30°08′ latitude, 108°47′–114°15′ longitude), bounded by Jiangxi in the east, Chongqing and Guizhou Province in the west, Guangdong and Guangxi in the south, and Hubei in the north. Hunan is mountainous and hilly in the east, west, and south. It is hilly with basins in the center and plains in the north. Its central and northern parts form a low and U-shaped basin facing north, with Dongting Lake as its center. Huping Mountain in Shimen County, Changde, is its highest mountain, with an elevation of 2,009 m. Its lowest point is in Huanggai Town, Yueyang at only 21 meters above sea level. It has a total area of 218,000 km^2 as shown in Figure 1.

Hunan is located in the transition from the Yunnan–Guizhou Plateau to the Jiangnan Hill and the Nanling Mountains to the Jianghan Plain. The terrain is a horseshoe-shaped landform that is surrounded by mountains. It consists of plains, basins, hills, mountains, rivers, and lakes. It crosses the Yangtze River and the Pearl River and has a subtropical monsoon climate. The average annual temperature (10–18.5 °C) is low in the southwest, high in the southeast, and high in the south and low in the north. The average monthly temperature is the highest in July at generally 20–30 °C, while it is the lowest in January at 2–7 °C. The maximum and minimum extreme temperatures are 43.7 °C (August 7, 1951, Yongzhou, Hunan) and −18.1 °C (January, 1969, Linxiang, Hunan), respectively. The multi-year average annual relative humidity is 78–84%. The relative humidity of mountains in the east, west, and south is higher than that in the hilly area of central Hunan. The frost-free period is 240–300 days, decreasing from south to north.

The average annual precipitation of the Dongting Lake water system is 1,200–2,000 mm, with an uneven spatio-temporal distribution. The average annual precipitation in the Congshan area of Hunan is 1,600–2,000 mm. The average annual precipitation in central Hunan and the Dongting Lake area is 1,200–1,300 mm. The maximum and minimum extreme annual precipitations are 3,697.4 mm (1998, Badagongshan station, Hunan Province) and 529.0 mm (1981, Zijingguan station, Guizhou Province), respectively. The average annual water surface evaporation is 600–1,000 mm, decreasing from the upper reaches of the Xiangjiang River to the upper and middle reaches of the Yuanjiang River and the Zishui River and the upper reaches of the Lishui River. The frequency of extreme continuous rainstorm events is increasing, and the intensity is aggravated. Generally, the extreme continuous rainstorms presented variations in three quasi-periods of 2–3a, 5–7a, and 12–16a. The increase of extreme continuous rainstorms is characterized by abrupt changes from the 1990s to early 2000s (Zhang *et al.* 2012).

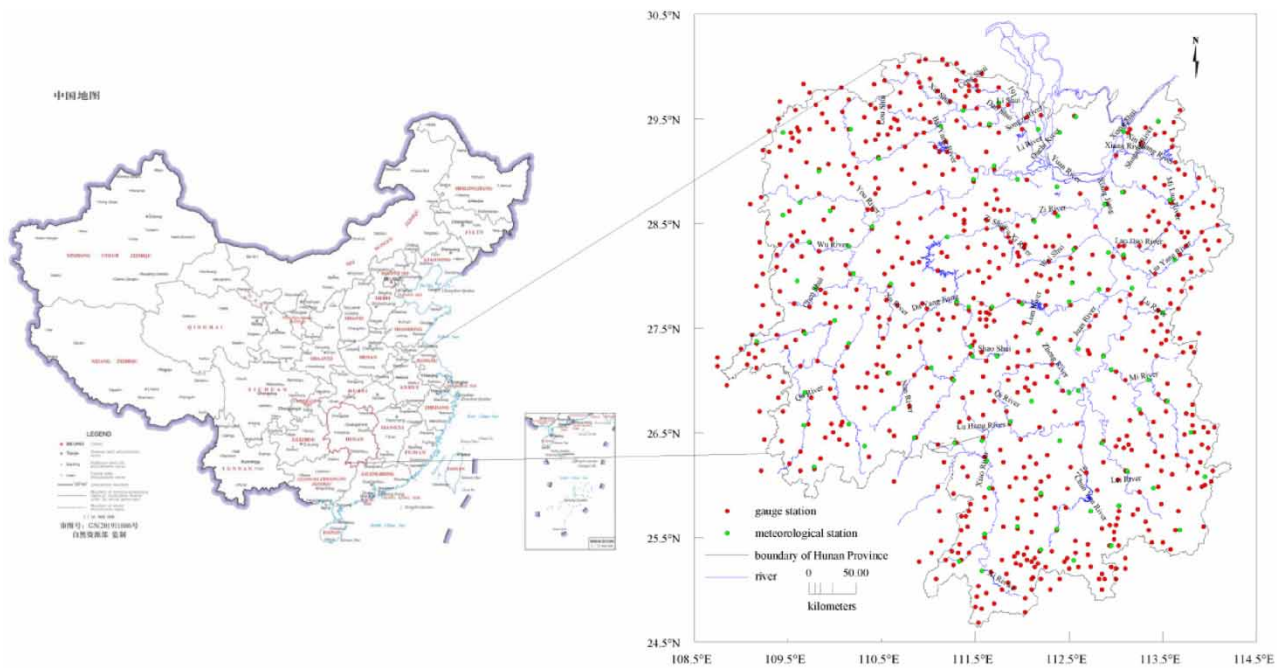

Figure 1 | Location of the study area and locations of meteorological stations.

2.2. Data

2.2.1. Extreme precipitation frequency and MT

As precipitation exhibits a wide spatial variation in Hunan Province, extreme precipitation must also exhibit spatial variations. Accordingly, the flood control facilities, flood control capacity, and flood precipitation are also spatially variable. Therefore, the most popular percentile method is used to define the extreme precipitation threshold and then to detect extreme precipitation events. For the determination of the percentile value, refer to the calculation method of Bonsal *et al.* (2001). The precipitation sequence of each station is arranged in ascending order, and the 90% percentile value is defined as the threshold value of extreme precipitation events. For analyzing extreme precipitation events and MT in Hunan Province from 1960 to 2009, 593 gauge stations for precipitation data and 97 meteorological stations for temperature data were used. In this study, the definition of precipitation process proposed by Zou *et al.* (2009) was applied: for each station, from the beginning of rainy days to the interruption of rainy days, if a rainfall event lasts for 2 or more days, it is defined as a precipitation process. At each station, when a certain precipitation process exceeds the threshold value of extreme precipitation, it is called an extreme precipitation event.

2.2.2. Climate data

Regarding climate data, potential height, wind speed, specific humidity, surface pressure, and temperature provided by the American National Center for Environment Prediction (NCEP), which can be downloaded from http://www.ncep.noaa.gov/, were used for the analysis. The resolution of the data was 2.5° × 2.5°. Precipitation data covering 1961–2009 were compiled from hydro-meteorological stations in Hunan Province.

2.3. Analysis methods

2.3.1. SVD method

The SVD method (Ghajarnia *et al.* 2016) is an important tool for analyzing the coupling and correlation of two element fields. It can be used to analyze the spatial structure of the correlation coefficient field between two fields and their respective contributions to the correlation field, which is more effective compared with the simple Pearson correlation coefficient. SVD is a general tool in the diagnosis of coupling correlations of temporal and spatial distributions of meteorological fields. Therefore, it is widely used in the diagnosis, analysis, and prediction of meteorological and climatic factors (Nastaran *et al.* 2016). The principle of SVD is as follows:

For example, take two fields X and Y, termed left and right fields, respectively. The left field has p space points (or the number of variables) and N observations. The right field has q space points (which can be different from p) and N observations, as shown in the following equation:

$$X_{p\times N}=\begin{pmatrix} x_{11} & x_{12} & \cdots & x_{1N} \\ x_{21} & x_{22} & \cdots & x_{2N} \\ \vdots & \vdots & \cdots & \vdots \\ x_{p1} & x_{p2} & \cdots & x_{pN} \end{pmatrix} \quad Y_{q\times N}=\begin{pmatrix} y_{11} & y_{12} & \cdots & y_{1N} \\ y_{21} & y_{22} & \cdots & y_{2N} \\ \vdots & \vdots & \cdots & \vdots \\ y_{q1} & y_{q2} & \cdots & y_{qN} \end{pmatrix} \tag{1}$$

By SVD decomposition, two orthogonal linear transformation matrices L and R can be found in the following equation:

$$A_{p\times q}=XY^T=L_{p\times p}\Lambda_{p\times q}R^T_{q\times q} \tag{2}$$

where L, Λ, and R represent the left and right singular matrices and a non-zero diagonal matrix of singular values of the original matrix, respectively; $U_{p\times N}=L^T_{p\times p}X_{p\times N}$ is called the temporal expansion series (TES) of the left field; and $V_{q\times N}=R^T_{q\times q}Y_{q\times N}$ is the TES of the right field.

The Squared Covariance Fraction (SCF) for each mode is computed in the following equation:

$$SCF=\frac{s^2_{i,i}}{\sum\limits_{i=1}^{\min(p,q)} s^2_{i,i}} \tag{3}$$

where $\boldsymbol{s}$ is the vector of diagonal eigenvalues from the diagonal values of Λ.

When analyzing the coupling correlation of the two element fields, it is necessary to determine the key area of the interaction between the two fields. Therefore, the anisotropic correlation coefficient needs to be calculated. To perform trend analysis, the data of the two fields were normalized using the Z-score normalization method. The heterogeneous correlation coefficient (HCC) function is defined in the following equation:

$$r_k(X, V) = \frac{E[x_i(t)V_k(t)]}{E(x_i^2(t))^{1/2}E(V_k^2(t))^{1/2}} \qquad r_k(Y, U) = \frac{E[y_i(t)U_k(t)]}{E(y_i^2(t))^{1/2}E(U_k^2(t))^{1/2}} \tag{4}$$

The HCC indicates the general influential regions of one field on the other field in a certain mode k, which can form a heterogeneous correlation field. The significant correlation area is the most critical area of the field affecting another field in the k mode.

The correlation coefficient r_k (U, V) between the TES corresponding to the kth pair of singular vectors represents the degree of correlation between the two coupled spatial distributions. The calculation formula of r_k (U, V) is defined in the following equation:

$$r_k(V, U) = \frac{E[V_k(t)U_k(t)]}{E(V_k^2(t))^{1/2}E(U_k^2(t))^{1/2}} \tag{5}$$

2.3.2. Calculation of water vapor transportation

Water vapor transportation refers to the water vapor content flowing through a unit cross-sectional area per unit time, which can be divided into horizontal water vapor transportation and vertical water vapor transportation. It reflects the path and intensity of water vapor transported from one area to another by airflow. This study focused on the path and intensity of water vapor transport and analyzed only horizontal water vapor transportation. The calculation formula is defined in the following equation:

$$F = g^{-1}\int_{p_z}^{p_s} qVdp \tag{6}$$

where V is the wind vector, which can be divided into zonal wind u and meridional wind v. It is stipulated that u is positive to the east, negative to the west, and v *is* positive to the north and negative to the south. q is specific humidity ($\mathrm{kg \cdot kg^{-1}}$), p_s is the surface air pressure, p_z is the air pressure at height Z, and g is the acceleration of gravity. The symbol of water vapor transportation is consistent with the direction of wind, and the unit is $\mathrm{kg \cdot m^{-1} \cdot s^{-1}}$.

2.3.3. Calculation of water vapor transportation divergence

The divergence of water vapor transportation represents the convergence and divergence of water vapor in a region. Because the National Centers for Environmental Prediction/American National Center for Environment Prediction (NECP/NCAR) reanalysis data are stored in the form of grids, it is more appropriate to use the latitude–longitude grid method to calculate the plane divergence. The formula for calculating water vapor transportation divergence is as follows:

$$D = \frac{1}{g}\nabla(Vq) = \frac{\partial}{\partial x}\left(\frac{1}{g}uq\right) + \frac{\partial}{\partial y}\left(\frac{1}{g}vq\right) \tag{7}$$

When the plane divergence is calculated by the latitude–longitude grid, as the latitude circle of the Earth decreases with an increasing latitude, the area of the latitude–longitude grid decreases the increasing latitude, which will result in a divergence increment as follows:

$$D' = -\frac{vq}{R_e}tg\varphi \tag{8}$$

where R_e is the radius of the Earth and φ is the latitude of the center point of the longitude–latitude grid.

After considering the revised term, the calculation formula of the divergence of water vapor transportation is discretized in the following equation:

$$D = \frac{1}{g}\left(\frac{(uq)_B - (uq)_A}{R_e \cos\varphi_0 \Delta\lambda} + \frac{(vq)_B - (vq)_A}{R_e \Delta\varphi} - \frac{(vq)_0}{R_e} tg\varphi_0\right) \tag{9}$$

where g is the acceleration of gravity, φ is the latitude, λ is the longitude (radian value), R_e is the radius of the earth, u is the zonal wind, v is the meridional wind, and q is the specific humidity. O is the center point of the mesh; A, B, C, and D are the center points of the mesh boundary curves (as shown in Figure 2), and their values represent the values of the entire boundary. The divergence of water vapor transportation can be calculated and analyzed using formula (9). Positive divergence represents water vapor convergence and negative divergence represents water vapor divergence. The unit of integral divergence of water vapor transportation is kg/(m^2·s).

3. RESULTS

3.1. Coupling relationship between extreme precipitation events and MT

Taking the MT of Hunan Province as the left field and the extreme precipitation frequency (EPF) as the right field, the SVD analysis was performed for the standardized average temperature series and standardized precipitation series covering four time periods (Year, Spring, Summer, and Autumn). The square covariance contribution rate and the correlation coefficient of the first three pairs of modes of the four types of coupling correlation analysis are shown in Table 1. The cumulative square covariance contribution rates of the first three pairs of modes were more than 70.3%, which indicates that the first three

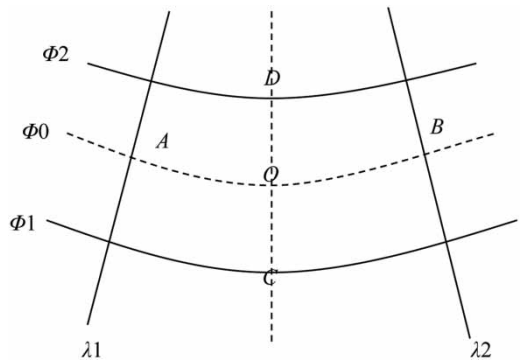

Figure 2 | Diagram of grid points for calculating divergence.

Table 1 | SCF and correlation coefficient of the first three pairs of modes for the four time periods

Time	Modes	SCF (%)	Cumulative SCF of the first three modes (%)	Correlation coefficient
Spring	First mode	47.9	47.9	0.801
	Second mode	19.5	67.4	0.848
	Third mode	11.8	79.2	0.915
Summer	First mode	32.7	32.7	0.898
	Second mode	21.7	54.4	0.924
	Third mode	15.9	70.3	0.931
Autumn	First mode	49.0	49.0	0.826
	Second mode	14.1	63.1	0.843
	Third mode	11.4	74.5	0.894
Year	First mode	60.6	60.6	0.852
	Second mode	11.7	72.3	0.884
	Third mode	8.1	80.4	0.836

modes represent most of the information of the coupling correlation between the two element fields. The correlation coefficients of each pair of modes were more than 0.80 and passed the significance level of 0.99, which shows that the correlation between each pair of modes is very significant.

The spatial distribution of HCC of the first-mode SVD of MT and EPF for Year, Spring, Summer, Autumn, and the corresponding TES are shown in Figure 3. The TES of the first-mode SVD of MT and EPF in Year (a), Spring (b), Summer (c), and Autumn (d) are shown in Figure 4.

Figure 3(a) shows a positive variation in Hunan, and almost all areas showed a significant correlation (HCC value greater than 0.4), especially in the eastern and western regions of Hunan Province with HCC values of up to 0.6. Figure 3(b) shows higher HCC values in the east and lower values in the west. Negative correlations were generally observed in Huaihua, Xiangxi, and Zhangjiajie, whereas other areas mainly showed positive correlations. The TES (Figure 4(a)) of the two fields exhibited the same trend, and the mode correlation coefficient was approximately 0.852. The TES of the first mode of the two fields showed a sudden change from the negative phase to the positive phase in 1987. This shows that under the situation of general warming in Hunan Province, the total EPF increases, but it decreases in Huaihua, Xiangxi, and Zhangjiajie.

Figure 3(c) shows negative HCC of EPF in spring, and the HCCs of the entire eastern region and northwest region were below −0.6. Figure 3(d) shows negative HCC of precipitation in spring in Western Hunan, Zhangjiajie, Changde, and Yueyang, and positive HCC in most of the other areas. The TES (Figure 4(b)) of the first mode of the two fields exhibited a consistent trend, indicating that since 1995, temperature in spring in Hunan Province has been decreasing, and the frequency of extreme precipitation events has been increasing in Western Hunan, Zhangjiajie, Changde, and Yueyang and decreasing in most of other areas of Hunan Province.

In Summer, the HCC of MT (Figure 3(e)) was negative in all regions, except Yongzhou and Chenzhou, especially in Xiangxi, Zhangjiajie, Changde, and Yueyang where HCC values were smaller than −0.4. The HCC of EPF (Figure 3(f)) was negative in central and southern Hunan Province, but positive in Western Hunan, Zhangjiajie, Changde, and Yueyang. The TES of the first mode of TM and EPF (SVD fields) were consistent, with a mode correlation coefficient of 0.826. The TES (Figure 4(c)) changed from positive to negative in 1992. These distribution patterns show that when TM increases in some areas of Yongzhou and Chenzhou and decreases in other areas in Summer, EPF increases in most areas of Xiangxi, Zhangjiajie, Changde, and Yueyang but decreases in other areas.

In Autumn, the HCC values of MT (Figure 3(g)) and EPF (Figure 3(h)) were positive and negative, respectively, except for Xiangtan and Changsha. The spatial distributions of HCC indicate that the EPF decreases with increasing MT. The TES (Figure 4(d)) of MT and EPF fields were almost consistent, and mutations in both occurred around 1988, and the first mode correlation coefficient was as high as 0.80.

3.2. Correlation analysis of temperature and extreme precipitation before and after abrupt changes

Figure 4 shows that the TES of the MT and EPF fields exhibit prominent mutations in the 1980s–1990s. Using the composite analysis method, MT and EPF before and after the mutation were synthesized, and the relationship between MT and EPF was further discussed. The time series from 1956 to 2016 was divided into two parts from the mutation points. Fields of differences in MT and EPF (values of MT and EPF after the mutation minus those before the mutation) are shown in Figure 5. The difference field of MT in Year (Figure 5(a)) showed positive differences, especially in Changde, Yiyang, Yueyang, Changsha, Xiangtan, Hengyang, Chenzhou, and Zhuzhou where temperature was higher by more than 0.4° after the mutation. The difference field of EPF (Figure 4(b)) exhibited a bipolar pattern from west to east. The distributions in Figures 3(a) and 3(b) and 5(a) and 5(b) are very similar, suggesting that the first mode of SVD can represent the real synergy change characteristics of the two fields.

In Spring (Figure 5(c) and 5(d)), TM was higher after the mutation in most areas of Hunan Province, and TM was higher in the central part than in the east and west. Compared with TM, the distribution of the difference field of EPF exhibited obvious regional differences. After the mutation, the value of the EPF increased in Changde and Yueyang (north of Hunan Province) and Chenzhou (south of Hunan Province), but it decreased in other areas. The spatial distributions in Figures 5(c) and 5(d) and 3(c) and 3(d) are similar, suggesting that the collaborative change of Spring MT and EPF can represent the real response of regional-scale EPF to climate warming.

The distributions of difference fields of MT and EPF in Summer are shown in Figure 5(e) and 5(f). The results show that the difference field of MT has a quadrupole distribution pattern of '+ −+ −' from southwest to northeast. After the mutation, MT was higher in Changde, Yiyang, Yueyang, Changsha, Xiangtan, Hengyang, Chenzhou, and Zhuzhou but lower in other areas. Comparing Figures 3(e) and 3(f) and 5(e) and 5(f), their distributions are basically the same.

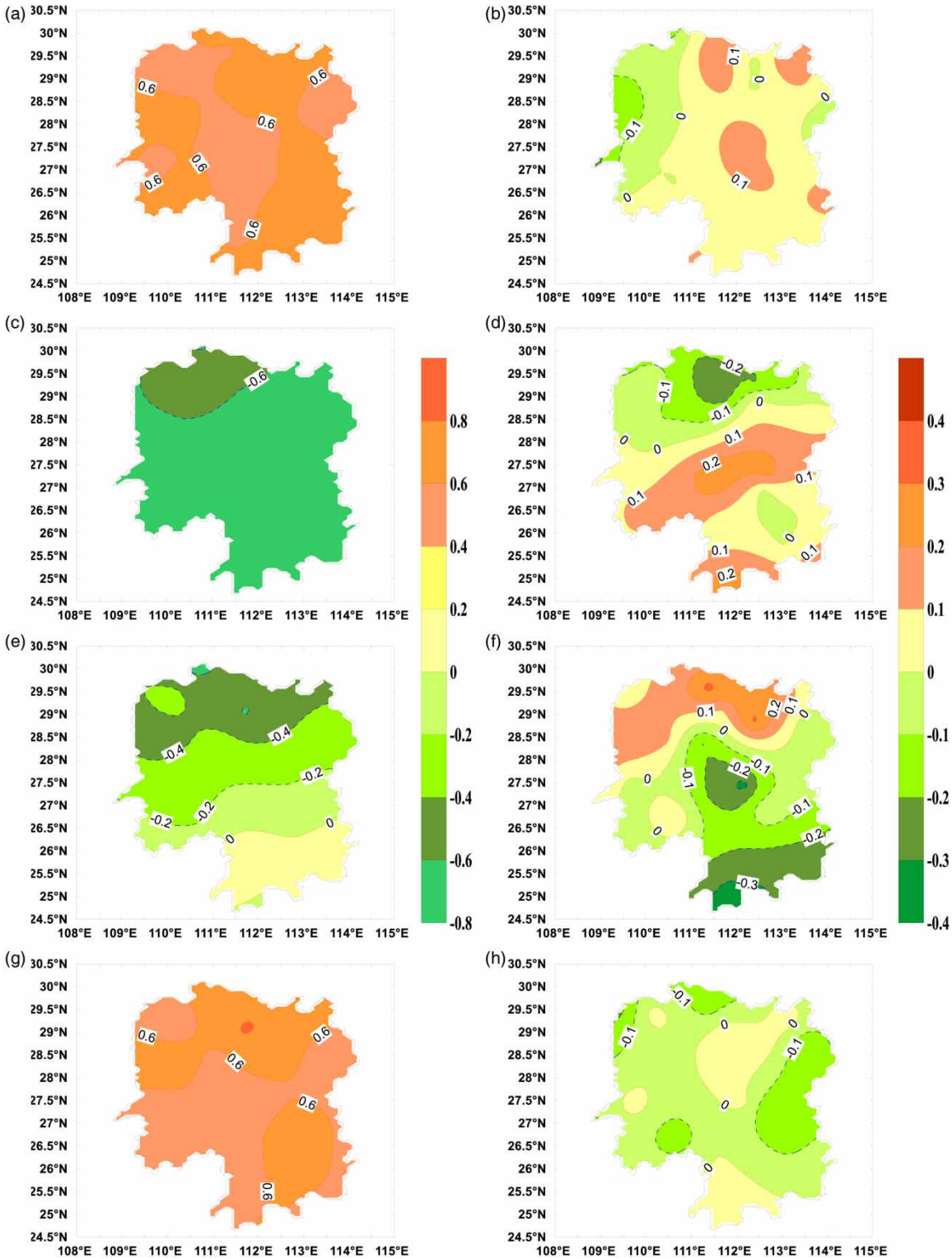

Figure 3 | Spatial distribution of the HCCs of the first-mode SVD of MT (a, c, e, g) and EPF (b, d, f, h) in Year, Spring, Summer, and Autumn.

The difference field of MT showed a consistent positive distribution in Summer (Figure 5(g)); EPF increased only in most areas of Yiyang and Xiangtan, and decreased in the remaining areas (Figure 5(h)). The distributions of HCC of the first-mode SVD of MT and EPF in Figure 3(g) and 3(h) are also similar to the distribution of difference fields in Figure 5(g) and 5(h).

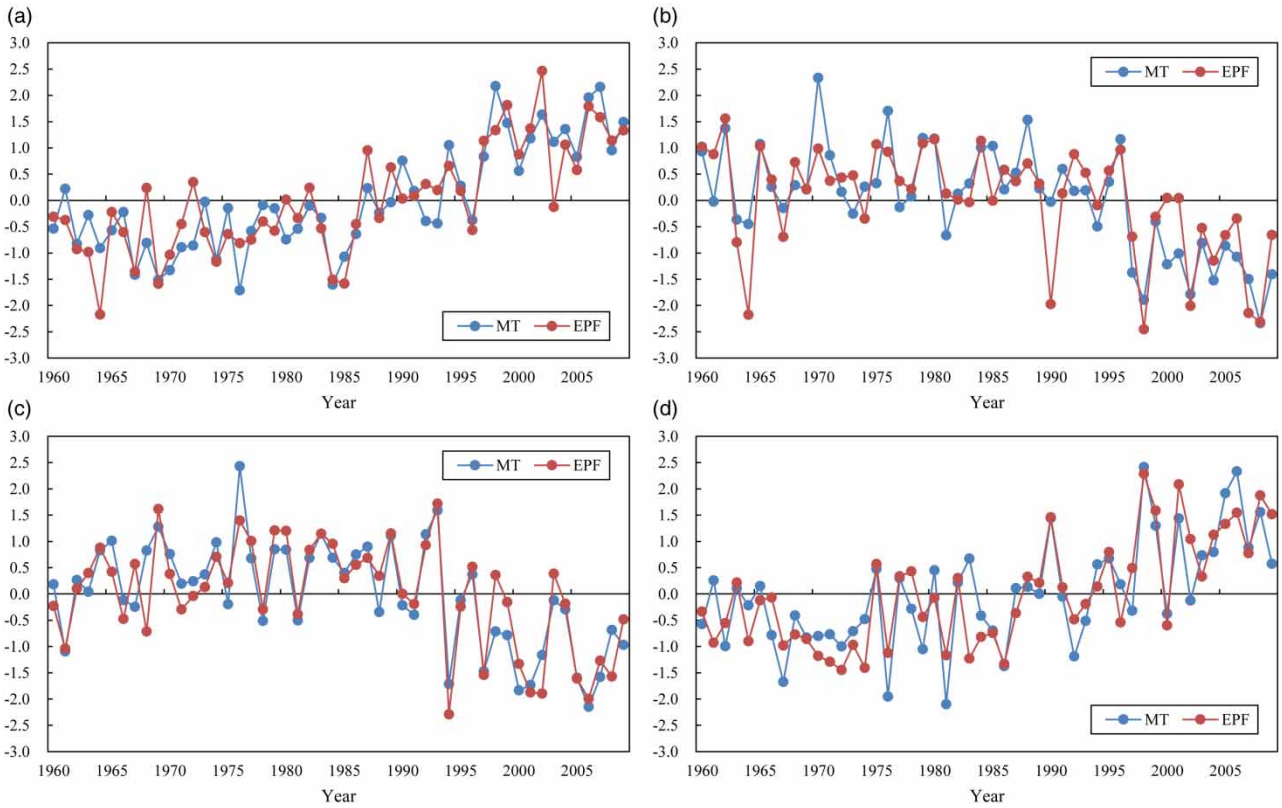

Figure 4 | TES of the first-mode SVD of MT and EPF in Year (a), Spring (b), Summer (c), and Autumn (d).

On the whole, MT (Year, Spring, Summer, and Autumn) exhibited a sudden warming mutation in the 1980s–1990s, but there were obvious regional and seasonal differences in the changes of EPF after the mutation. The frequency of extreme precipitation events increased in Spring and Autumn but decreased in Year and Summer, indicating more centralized extreme precipitation events in summer after the mutation. The synergy of HCC fields of the first-mode SVD and difference fields of MT and EPF can basically reflect the true response of extreme precipitation events to climate warming in Hunan Province.

3.3. Comparison of atmospheric circulation before and after abrupt changes

Prominent abrupt changes were observed in the TES of MT and EPF in Year, Spring, Summer, and Autumn. The climatic mutation is definitely related to atmospheric circulation. Therefore, to further analyze the cooperative relationship between MT and EPF, interdecadal differences in the corresponding large-scale atmospheric circulation before and after the mutation were investigated using the composite analysis method. Wind speed anomaly at 850 ha is generally considered to be the main atmospheric circulation characteristics affecting extreme precipitation events (Wu *et al.* 2018; Fang & Qiao 2019). Therefore, EPF was further analyzed considering wind anomalies (850 hPa), the entire layer of anomalous vapor transportation flux and divergence before and after the mutations in Year, Spring, Summer, and Autumn.

3.3.1. Anomalous wind

Fields of wind anomalies before and after the mutations in Year, Spring, Summer, and Autumn are shown in Figure 6.

Wind anomaly fields in Year showed prominent differences before and after the mutation (Figure 6(a) and 6(b)). Before the mutation, the northwest wind anomaly was strong, dry, and cold, which may lead to less extreme precipitation events. On the contrary, the southerly wind anomaly after the sudden change is strong, which can blow northward as far as northeast China and bring warm and humid air from the Southern Ocean to Hunan Province, resulting in more extreme precipitation events in some parts of Hunan Province.

Wind anomaly fields before and after the mutation in Spring, Summer, and Autumn are shown in Figure 6(c)–6(h). Wind anomaly fields before and after the mutation showed the opposite trends. Nevertheless, the wind anomaly fields were relatively consistent among the three seasons.

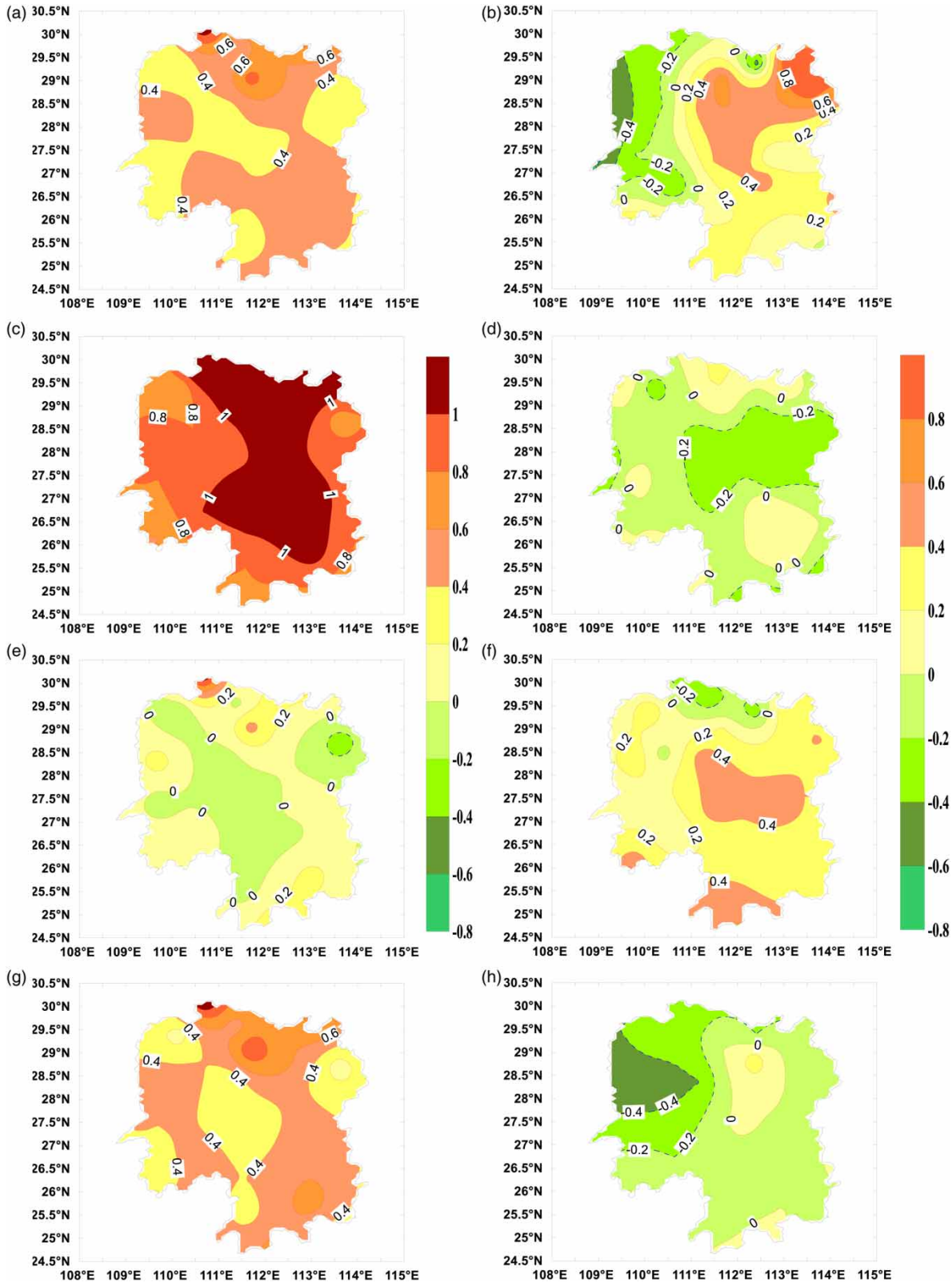

Figure 5 | Difference fields of MT (a, c, e, g) and EPF (b, d, f, h) before and after the mutation in Year, Spring, Summer, and Autumn.

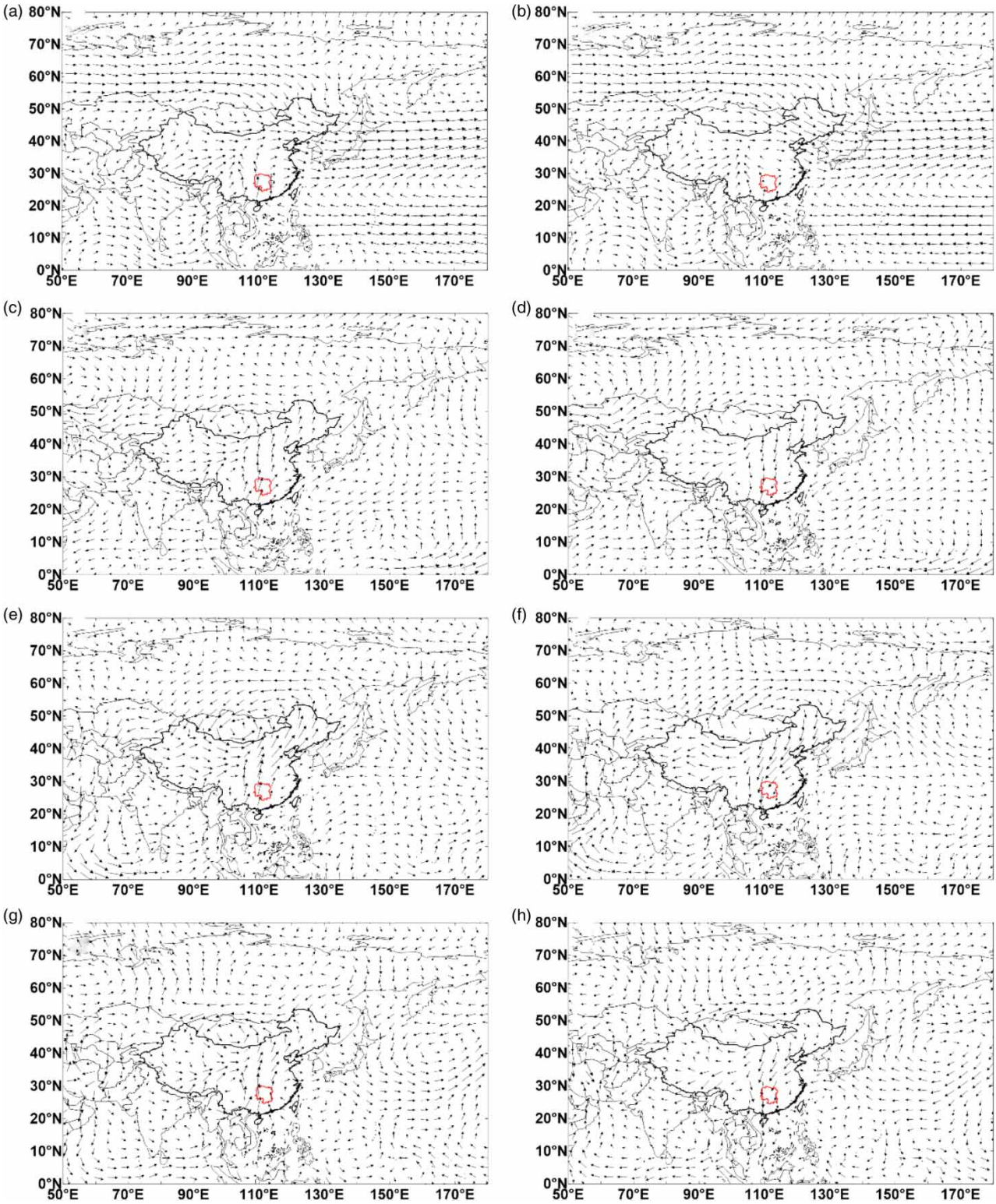

Figure 6 | Wind anomaly (850 hPa) fields before (a, c, e, g) and after (b, d, f, h) the mutation in Year, Spring, Summer, and Autumn.

Taking Summer as an example, the wind anomaly field before the mutation (Figure 6(e)) indicated an abnormal cyclone circulation in the center of Mongolia in the north of East Asia, which played a very important role in the cooling of Hunan Province by strengthening the southward inflow of cold air. Although southerly warm and humid air from the Bay

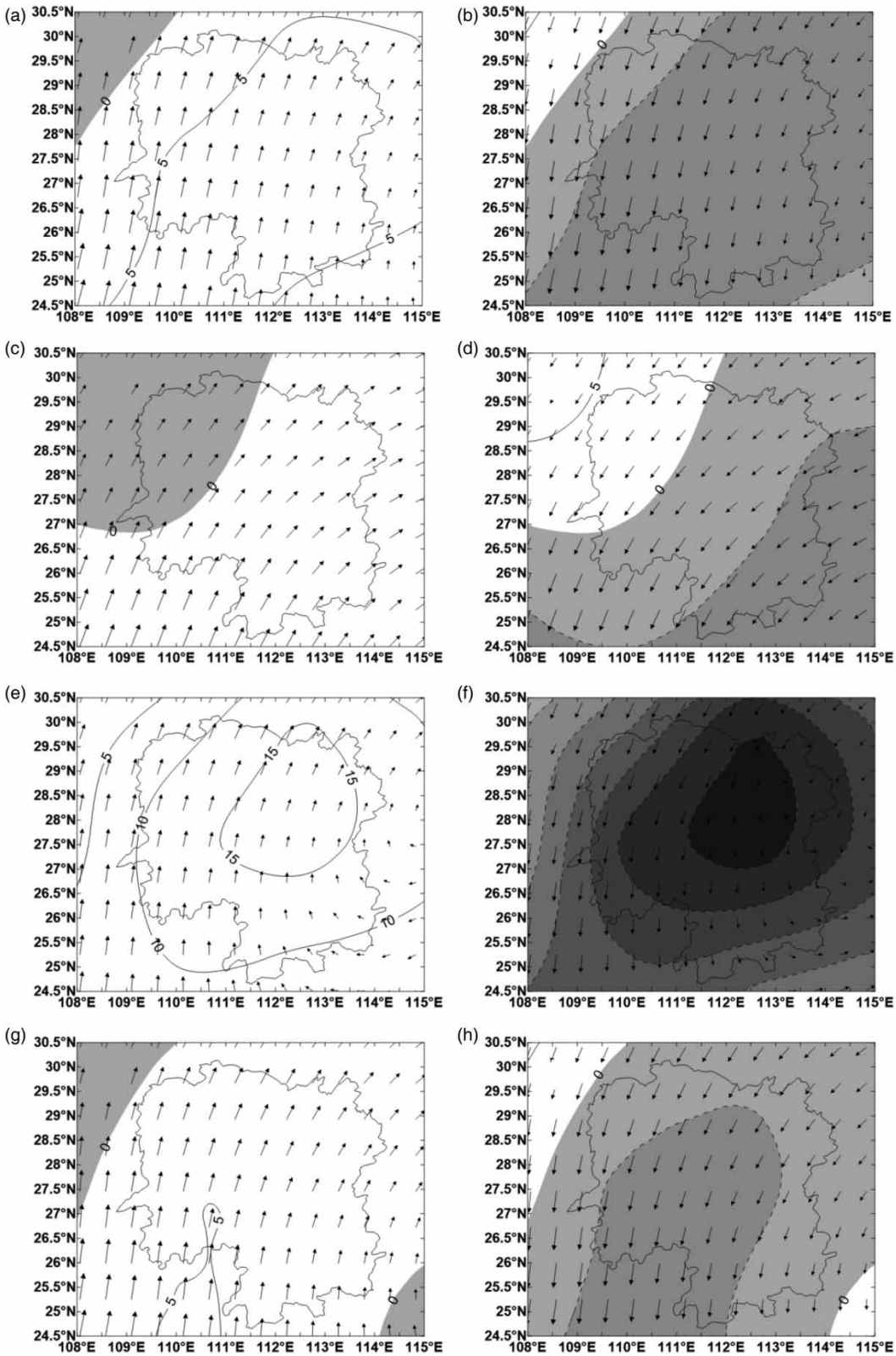

Figure 7 | Fields of anomalous water vapor flux (vector, kg·m^{-1}·s^{-1}) and divergence (isoline, shadow is convergence area, 10^{-5} kg/(m^2·s)) in the entire layer before (a, c, e, g) and after (b, d, f, h) the mutation in Year, Spring, Summer, and Autumn.

of Bengal in the Indian Ocean prevailed in Hunan Province, there was no convergence of cold and warm air. Thus, the value of EPF was low. However, after the mutation (Figure 6(f)), the wind anomaly field in Summer became opposite to that before the mutation, and an anticyclone developed in Mongolia, which significantly weakened cold air from northern to southern China, resulting in the high temperature in Hunan Province. Hunan Province is located in a cyclonic circulation, and the abnormal bottom convergence is conducive to precipitation, resulting in more extreme precipitation events.

3.3.2. Entire layer of anomalous vapor transportation flux and divergence

The fields of the entire layer of anomalous vapor transportation flux and divergence before and after the mutations in Year, Spring, Summer, and Autumn are shown in Figure 7.

The direction of vapor transportation and divergence showed prominent differences before and after the mutation. Water vapor transport before and after the mutation showed completely opposite trends irrespective of the period (Year, Spring, Summer, or Autumn).

Before the mutation, the anomalous water vapor divergence in Spring and Autumn was not conducive to water diversion, and thus, the frequency of regional extreme precipitation events was low. However, after the mutation, the water vapor convergence became conducive to water diversion, and thus, the frequency of regional extreme precipitation events increased. The abnormal water vapor divergence in Year and Summer was unfavorable for precipitation before the mutation, and thus, the frequency of regional extreme precipitation events was low. However, it became favorable for precipitation after the mutation, thus increasing the frequency of regional extreme precipitation events. Compared with water vapor convergence in Year, Spring, and Autumn, the water vapor convergence in Summer was the strongest after the mutation.

4. CONCLUSIONS AND DISCUSSION

The relationship between temperature and extreme rainfall events in Hunan Province over various time periods (Year, Spring, Summer, and Autumn) was investigated using the SVD method. The results showed that the first three modes represent the vast majority of the correlation between the two factors, with significant correlations between each mode. Furthermore, the relationship between extreme rainfall events in Hunan Province and sea surface temperature in different time periods was investigated. The following conclusions can be drawn:

1. The annual and Spring, Summer and Autumn MT in Hunan Province exhibited a sudden change during the 1980s–1990s. However, the trend of temperature change was widely varied among the four different periods, and the trend of extreme precipitation events before and after the sudden change exhibited prominent regional variations. In particular, the response of EPF to the average temperature in Hunan Province was more obvious in Spring and Summer, with significant regional differences. Especially in summer, the frequency of extreme rainfall events in some regions decreased significantly with an increasing temperature.
2. The correlation between MT and the frequency of extreme rainfall also exhibited a significant spatial variation before and after the mutation. The correlation was especially prominent in Spring before the mutation, but it weakened after the mutation. In some areas, the correlation changed from positive to negative.
3. Further analysis of the wind anomaly field (annual mean) before and after the abrupt change revealed that the wind anomaly field in Summer exhibited the opposite trends before and after the abrupt change, and the frequency of extreme precipitation events increased after the abrupt change. In Year and Summer, an anomalous convergence of northerly and easterly water vapor appeared after the abrupt change, increasing the frequency of extreme precipitation events. Wu *et al.* (2018) reported a similar result. They found that increases in the frequency of extreme precipitation always correspond to weaker than normal East Asian summer monsoon, which is reflected in abnormal 850-hPa wind field and water vapor flux that are favorable for more water vapor transport to the middle and lower reaches of Yangtze River.

The current research mainly discusses the change of atmospheric circulation under the condition of EPF anomaly in Hunan Province from the perspective of internal dynamics. However, the thermal condition of the atmosphere and other external forcing also have an important impact on the summer extreme precipitation events, which should be taken into account in the further study. Meanwhile, comparison between the SVD method and other methods needs to be strengthened. Furthermore, the hydrological prediction caused by extreme precipitation under climate change should be further studied (Zhao *et al.* 2018; Shahabbodin *et al.* 2020).

ACKNOWLEDGEMENTS

This work is supported by the Water Science and Technology Program of Hunan Province (Grant Nos. XSKJ2018179-42 and XSKJ2019081-09) and 'the Fundamental Research Funds for the Central Universities', South-Central University for Nationalities (Grant No. CZQ18022). Finally, the authors would like to thank the editor and anonymous reviewers for their helpful comments and suggestions.

CONFLICTS OF INTEREST

The authors declare no conflict of interest.

DATA AVAILABILITY STATEMENT

All relevant data are available from an online repository or repositories (http://data.cma.cn/).

REFERENCES

Ali, H., Fowler, H. J. & Mishra, V. 2018 Global observational evidence of strong linkage between dew point temperature and precipitation extremes. *Geophysical Research Letters* **45** (22), 12320–12330.

Allen, M. R. & Ingram, W. J. 2002 Constraints on future changes in climate and the hydrologic cycle. *Nature* **419**, 22.

An, D., Du, Y., Berndtsson, R., Niu, Z., Zhang, L. & Yuan, F. 2020 Evidence of climate shift for temperature and precipitation extremes across Gansu Province in China. *Theoretical and Applied Climatology* **139**, 1137–1149.

Baidya, S. K., Shrestha, M. L. & Sheikh, M. 2008 Trends in daily climatic extremes of temperature and precipitation in Nepal. *Journal of Hydrology and Meteorology* **5**, 38–51.

Berg, P., Haerter, J., Thejll, P., Piani, C., Hagemann, S. & Christensen, J. 2009 Seasonal characteristics of the relationship between daily precipitation intensity and surface temperature. *Journal of Geophysical Research: Atmospheres* **114**, D18102.

Bonsal, B. R., Zhang, X., Vincent, L. A. & Hogg, W. D. 2001 Characteristics of daily and extreme temperatures over Canada. *American Meteorological Society* **14**, 1959–1976.

Cai, J., He, Y., Xie, R. & Liu, Y. 2019 A footprint-based water security assessment: an analysis of Hunan province in China. *Journal of Cleaner Production* **118485**, 1–10.

Chen, J., Wu, X., Finlayson, B. L., Webber, M., Wei, T., Li, M. & Chen, Z. 2014 Variability and trend in the hydrology of the Yangtze River, China: annual precipitation and runoff. *Journal of Hydrology* **513**, 403–412.

Chen, J., Lu, G., Wu, Z., Gu, S. & He, H. 2016 Change properties of summer extreme precipitation events and temperature and associated large-scale circulation in China during 1960–2009. *Plateau Meteorology* **35** (3), 675–684.

Dai, A. G., Trenberth, K. E. & Karl, T. R. 1998 Global variation in droughts and wet spells: 1900–1995. *Geophysical Research Letters* **25**, 3367–3370.

Deng, H. & Chen, Y. 2017 Influences of recent climate change and human activities on water storage variations in Central Asia. *Journal of Hydrology* **544**, 46–57.

Douville, H., Ribes, A., Decharme, B., Alkama, R. & Sheffield, J. 2012 Anthropogenic influence on multidecadal changes in reconstructed global evapotranspiration. *Nature Climate Change* **3** (1), 59–62.

Fang, H. & Qiao, Y. 2019 Spatial temporal distribution and circulation background of summer extreme precipitation in eastern China. *Acta Tropical Meteorologica Sinica* **35** (4), 517–527.

Frich, P., Alexander, L. V., Della-Marta, P., Gleason, B., Haylock, M., Tank, AMGK & Peterson, T. 2002 Observed coherent changes in climatic extremes during the second half of the twentieth century. *Climate Research* **19**, 193–212.

Gao, X., Zhu, Q., Yang, Z., Liu, J., Wang, H., Shao, W. & Huang, G. 2018 Temperature dependence of hourly, daily, and event-based precipitation extremes over China. *Scientific Reports* **8**, 17564.

Gao, X., Guo, M., Yang, Z., Zhu, Q., Xu, Z. & Gao, K. 2020 Temperature dependence of extreme precipitation over mainland China. *Journal of Hydrology* **583**, 124595.

Gemmer, M., Becker, S. & Jiang, T. 2004 Observed monthly precipitation trends in China 1951–2002. *Theoretical and Applied Climatology* **77**, 39–45.

Ghajarnia, N., Arasteh, P., Araghinejad, S. & Liaghat, M. 2016 A hybrid Bayesian-SVD based method to detect false alarms in PERSIANN precipitation estimation product using related physical parameters. *Journal of Hydrology* **538**, 640–650.

Groisman, P., Karl, T., Easterling, D., Knight, R., Jamason, P., Hennessy, K., Suppiah, R., Page, C., Wibig, J., Fortuniak, K., Razuvaev, V., Douglas, A., Førland, E. & Zhai, P. 1999 Changes in the probability of extreme precipitation: important indicators of climate change. *Climatic Change* **42**, 243–283.

Guo, J., Guo, S., Li, Y., Chen, H. & Li, T. 2013 Spatial and temporal variation of extreme precipitation indices in the Yangtze River basin, China. *Stochastic Environmental Research and Risk Assessment* **27** (2), 459–475.

IPCC 2013 *Climate Change 2013: The Physical Science Basis Contribution of Working Group I to the Fifth Assessment Report of the Intergovernmental Panel on Climate Change*. Cambridge University Press, Cambridge, UK and New York, NY.

Jiang, T., Su, B. & Hartmann, H. 2007 Temporal and spatial trends of precipitation and river flow in the Yangtze River Basin, 1961–2000. *Geomorphology* **85** (3–4), 143–154.

Lü, M., Wu, S.-J., Chen, J., Chen, C., Wen, Z. & Huang, Y. 2018 Changes in extreme precipitation in the Yangtze River basin and its association with global mean temperature and ENSO. *International Journal of Climatology* **38** (4), 1989–2005.

Lupikasza, E. 2009 Spatial and temporal variability of extreme precipitation in Poland in the period 1951–2006. *International Journal of Climatology* **30**, 991–1007.

Manton, M. J., Della-Marta, P. M., Haylock, M. R., Hennessy, K. J., Nicholls, N., Chambers, L. E., Collins, D. A., Daw, G., Finet, A., Gunawan, D., Inape, K., Isobe, H., Kestin, T. S., Lefale, P., Leyu, C. H., Lwin, T., Maitrepierre, L., Ouprasitwong, N., Page, C. M., Pahalad, J., Plummer, N., Salinger, M. J., Suppiah, R., Tran, V. L., Trewin, B., Tibig, I. & Yee, D. 2010 Trends in extreme daily rainfall and temperature in Southeast Asia and the South Pacific: 1961–1998. *International Journal of Climatology* **21** (3), 269–284.

Nastaran, C., Ali, A. & Shahab, A. 2016 Pre-processing of data-driven river flow forecasting models by singular value decomposition (SVD) technique. *Hydrological Sciences Journal* **61** (12), 2164–2178.

Ning, L. & Qian, Y. 2009 Interdecadal change in extreme precipitation over South China and its mechanism. *Advances in Atmospheric Sciences* **26** (1), 109–118.

Oruc, S. 2021 Trend and nonstationary relation of extreme rainfall: central Anatolia, Turkey. *Acta Geophysica* **2A**, 1–13.

Pumo, D., Carlino, G., Blenkinsop, S., Arnone, E., Fowler, H. & Noto, L. V. 2019 Sensitivity of extreme rainfall to temperature in semi-arid Mediterranean regions. *Atmospheric Research* **225**, 30–44.

Shahabbodin, S., Sajjad, H. & Hana, S. 2020 Predicting standardized streamflow index for hydrological drought using machine learning models. *Engineering Applications of Computational Fluid Mechanics* **14** (1), 339–350.

Sharma, A. & Goyal, M. K. 2020 Assessment of the changes in precipitation and temperature in Teesta River basin in Indian Himalayan Region under climate change. *Atmospheric Research* **231**, 104670.

Singh, V. & Xiaosheng, Q. 2019 Data assimilation for constructing long-term gridded daily rainfall time series over Southeast Asia. *Climate Dynamics* **53**, 3289–3313.

Wang, Y. & Zhou, L. 2005 Observed trends in extreme precipitation events in China during 1961–2001 and the associated changes in large-scale circulation. *Geophysical Research Letters* **32**, L09707. doi:10.1029/2005GL022574.

Wang, W., Yang, X., Xie, Y., Zou, Y., Fang, J. & Xie, Q. 2012 Spatio-temporal variation of seasonal extreme wed days in China and its relationship with SST anomalies. *Journal of Tropical Meteorology* **18** (4), 485–493.

Wu, X., Chen, X., Tang, Y., Wang, Z. & Lai, C. 2015 Spatio-temporal variations and the causes of non-stationary extreme precipitation in the Pearl River basin. *Journal of Hydraulic Engineering* **46** (9), 1055–1063 (in Chinese).

Wu, W., You, Q., Wang, D. & Neng, R. 2018 Characteristics of extreme precipitation and associated anomalous circulations over eastern China during boreal summer. *Climatic and Environmental Research (in Chinese)* **23** (1), 47–58.

Wu, M., Wang, H., Wang, W., Song, Y., Ma, L., Lu, X., Wang, N. & Liu, C. 2020 The impact of heavy rain event on groundwater microbial communities in Xikuangshan, Hunan Province, P.R. China. *Journal of Hydrology* **22**, 125674.

Ye, X., Zhang, Q., Liu, J., Li, X. & Xu, C. 2013 Distinguishing the relative impacts of climate change and human activities on variation of stream flow in the Poyang Lake Catchment, China. *Journal of Hydrology* **494**, 83–95.

Zhang, Q., Singh, V. P., Sun, P., Chen, X. & Li, J. 2011 Precipitation and streamflow changes in China: changing patterns, causes and implications. *Journal of Hydrology* **410** (3), 204–216.

Zhang, J., Liao, Y., Duan, L. & Zeng, X. 2012 Climate variations of extreme continuous rainstorms in Hunan during 1960–2009. *Geographical Research* **31** (6), 1004–1015.

Zhang, Q., Li, J., Singh, V. P., Xu, C.-Y. & Deng, J. 2013 Influence of ENSO on precipitation in the East River basin, south China. *Journal of Geophysical Research: Atmospheres* **118** (5), 2207–2219.

Zhao, C., Huang, Y., Li, Z. & Chen, M. 2018 Drought monitoring of southwestern China using insufficient grace data for the long-term mean reference frame under global change. *Journal of Climate* **31** (17), 6897–6911.

Zou, Y., Yang, X., Sun, J., Fang, J. & Liao, Y. 2009 Seasonal difference of the spatio-temporal variation of the number of the extreme precipitation processes in China. *Journal of Nanjing University* **45** (1), 98–109 (in Chinese).

First received 18 May 2021; accepted in revised form 24 August 2021. Available online 7 September 2021